# Nanocasting Hierarchical Carbide-Derived Carbons in Nanostructured Opal Assemblies for High-Performance Cathodes in Lithium–Sulfur Batteries

**Claudia Hoffmann,[†] Sören Thieme,[‡] Jan Brückner,[‡] Martin Oschatz,[†] Tim Biemelt,[†] Giovanni Mondin,[†] Holger Althues,[‡] and Stefan Kaskel*[,†,‡]**

[†]Department of Inorganic Chemistry, Dresden University of Technology, Bergstrasse 66, 01069 Dresden, Germany and [‡]Fraunhofer Institute for Material and Beam Technology Winterbergstraße 28, 01277 Dresden, Germany

**ABSTRACT** Silica nanospheres are used as templates for the generation of carbide-derived carbons with monodisperse spherical mesopores ($d = 20-40$ nm) and microporous walls. The nanocasting approach with a polycarbosilane precursor and subsequent pyrolysis, followed by silica template removal and chlorine treatment, results in carbide-derived carbons DUT-86 (DUT = Dresden University of Technology) with remarkable textural characteristics, monodisperse, spherical mesopores tunable in diameter, and very high pore volumes up to 5.0 $cm^3\ g^{-1}$. Morphology replication allows these nanopores to be arranged in a nanostructured inverse opal-like structure. Specific surface areas are very high (2450 $m^2\ g^{-1}$) due to the simultaneous presence of micropores. Testing DUT-86 samples as cathode materials in Li–S batteries reveals excellent performance, and tailoring of the pore size allows optimization of cell performance, especially the active center accessibility and sulfur utilization. The outstanding pore volumes allow sulfur loadings of 80 wt %, a value seldom achieved in composite cathodes, and initial capacities of 1165 mAh $g_{sulfur}^{-1}$ are reached. After 100 cycle capacities of 860 mAh $g_{sulfur}^{-1}$ are retained, rendering DUT-86 a high-performance sulfur host material.

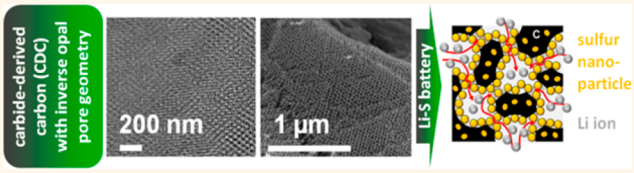


**KEYWORDS:** small-angle X-ray scattering · DUT-86 · carbide-derived carbon · lithium–sulfur battery · inverse opal

Nanoporous carbons play a key role in various fields such as adsorption,[1] gas storage,[2] catalysis,[3,4] biochemistry,[5] and electronics.[6−9] Generating hierarchical porosity into carbons is required for several applications such as enzyme immobilization or electrodes for fuel cells.[10] Typical procedures frequently used for generating porosity are treatment of carbons with gaseous oxidizing agents (*e.g.*, air and $CO_2$) known for physical activation[11,12] and the use of chemical agents (*e.g.*, KOH and $H_3PO_4$) for chemical activation.[13] Furthermore, nanocasting is a key technique to synthesize nanostructured materials by using hard templates as a kind of mold for shaping a precursor and performing the transformation to the desired product, especially in the range of 3–1000 nm. Subsequent removal of the template results in casted porosity.[14] Carbide-derived carbons (CDCs) on the other hand are high-performance adsorbents with tunable porosity due to the impact of the precursor and adjustable synthesis conditions.[15,16] The metal atoms are selectively extracted from the carbide structure by treatment in hot halogens, leading to the formation of microporous carbon materials ($d < 2$ nm) with narrow pore size distribution. The type of metal in the carbide (*e.g.*, Ti, Al, or Si) and the temperature of halogen treatment are crucial for the adjustable pore sizes and the porosity especially below 2 nm. Hence, the combination of the two concepts—nanocasting and CDC—allows nanostructure and pore structure control for carbons at different length scales. Several silicon carbide-derived carbons have been synthesized by applying the nanocasting process and yielding carbons with hierarchical porosity (micro- and mesoporous). Ordered mesoporous silica templates such as SBA-15[3] and KIT-6[17] and also disordered ones like a mesocellular siliceous foam[18] have been used. The resulting CDCs exhibit exceptionally high specific surface areas up

* Address correspondence to stefan.kaskel@chemie.tu-dresden.de.

Received for review June 23, 2014 and accepted November 29, 2014.

**Published online November 29, 2014**
**10.1021/nn503394u**

to 2900 $m^2\ g^{-1}$ and pore volumes of 2.6 $cm^3\ g^{-1}$. The mesoscopically ordered CDCs are characterized by the presence of mesopores with diameters of 4−5 nm. While those carbide-derived carbons have mainly convex mesopore walls, it was demonstrated that carbons with concave pores can be suitable, for example, for adsorption of dyes,[19] electrochemical energy storage applications (Li−S batteries[20−26] and electric double-layer capacitors[27,28]), optical devices,[29,30] space-confined synthesis of zeolite particles,[31] and as a catalyst support.[32] To the best of our knowledge, hierarchical carbide-derived carbons with concave nanopore walls and precisely defined spherical nanopores have not yet been described in the literature. However, those systems could have beneficial features for the stated applications due to the presence of additional microporosity.

Hence, the aim of the presented work is to synthesize CDC with interconnected spherical pores on the nanoscale arranged in an inverse opal-like manner in combination with microporous walls. We describe the size control of the monodisperse spherical pores as well as the interconnecting window pores of the carbide-derived carbons (DUT-86; DUT = Dresden University of Technology) by applying uniformly sized silica nanospheres as templates in a nanocasting approach. Furthermore, the DUT-86 samples are investigated regarding their applicability as conductive sulfur host materials in Li−S batteries, which are a highly promising future alternative to the state-of-the-art lithium ion technology. Although the main advantages, such as intrinsic overcharge protection,[33] great abundance, low-cost raw materials, as well as a huge increase in energy density,[34,35] which is attributable to the theoretical cathode active material capacity of impressive 1672 mAh $g_{sulfur}^{-1}$, are on hand, the system still does not meet the commercialization requirements. Among others, low active material (sulfur) utilization, the limited number of reversible charge/discharge cycles, and a low Coulombic efficiency (CE) of the Li−S cell count as the major drawbacks. Interestingly, all the mentioned hurdles are rooted in the complex electrochemical conversion of sulfur proceeding *via* a multistage multiphase reaction of soluble lithium polysulfides and solid sulfur as well as lithium sulfide species within the cathode layer.[36,37] This highlights the close relationship between cell performance and cathode structure or, in more detail, properties of both the conductive (porous) carbon additive and the carbon/sulfur composite prepared thereof.[21,38−40] Consequently, the application of tailored carbon structures with special pore characteristics and high surface areas in carbon/sulfur composites[22,25,41−44] and the surface modification of these composites by thin film coating[45−48] are highly promising approaches to increase the electrical contact to insulating precipitates (high sulfur utilization), compensate occurring volume changes, and improve the active material retention (long-term cyclability and high CE).

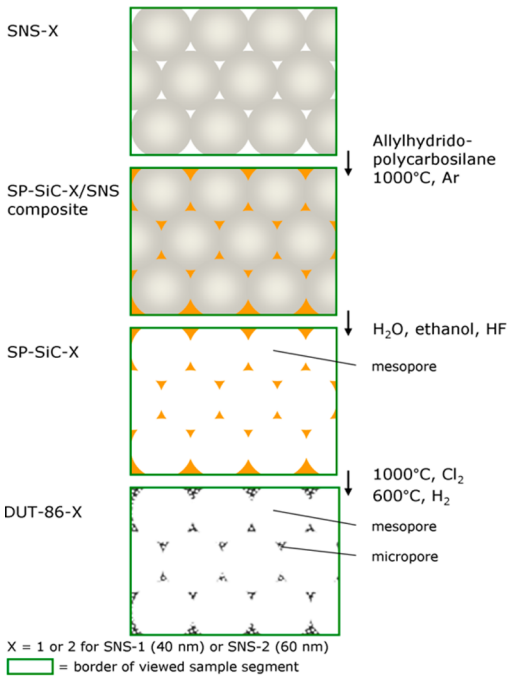


**Figure 1. Synthesis scheme from the parent silica nanospheres (SNS-X) to nanoporous silicon carbides (SP-SiC-X) and further to carbide-derived carbon materials (DUT-86-X) for X = 1 or X = 2 with silica sphere size of 40 or 60 nm, respectively. White parts symbolize pores.**

## RESULTS AND DISCUSSION

**Structure and Porosity of CDC with Spherical Nanopores (DUT-86) and Its Composites with Sulfur.** *Carbide-Derived Carbons (DUT-86) and Their Parent Silicon Carbides.* Silicon carbides with spherical pores (SP-SiC-1 and SP-SiC-2) have been synthesized *via* nanocasting of silica nanospheres (40 and 60 nm in diameter), as shown in Figure 1.

After selective removal of the siliceous material present in the silicon carbide/template composite obtained after pyrolysis of the polycarbosilane SMP-10 infiltrated $SiO_2$, nitrogen physisorption isotherms of type IV according to the IUPAC classification can be determined for SP-SiC-1 (SP = spherical pore) and SP-SiC-2 (Supporting Information, Figure S1). The hysteresis loops are of type H1, and steep slopes of adsorption and desorption branches are characteristic, resulting in pore size distributions as shown in Figure S2. As described in earlier publications,[49,50] depending on the branch used, the size of the spherical nanopores $d_{P,BJH}$ (adsorption branch; induced by the sphere templates SNS-1 and SNS-2) or the connecting window pores $d_{w,BJH}$ (desorption branch; contact faces of the spheres during nanocasting process) can be calculated using the BJH method, and results are summarized in Table 1. It should be emphasized that the sphere pore diameter for SP-SiC-2 only represents an estimation because the BJH method should only be applied for

**TABLE 1. Properties of the Parent Silicon Carbides, Carbide-Derived Carbons DUT-86 and DUT-86/S Composites Determined from Nitrogen Physisorption and Small-Angle X-ray Scattering Experiments**

| sample | $S_{BET}$ [a] ($m^2/g$) | $V_p$ [b] ($cm^3/g$) | $V_{micro}$ [c] ($cm^3/g$) | $d_{P,BJH}$ [d] (nm) | $d_{w,BJH}$ [e] (nm) | $d_{P,SAXS}$ [f] (nm) | $d_{SNS,SAXS}$ [f] (nm) |
|---|---|---|---|---|---|---|---|
| SP-SiC-1 | 657 | 2.15 | 0.06 | 34.1 | 11.6 | 33.8 | 40.8 |
| DUT-86-1 | 2392 | 3.66 | 0.50 | 18.2 | 9.1 | 22.4 | 40.8 |
| DUT-86-1/S | 47 | 0.18 | 0.00 | 18.0 | 8.1 | | 40.8 |
| SP-SiC-2 | 518 | 2.01 | 0.06 | 68.3 | 19.4 | 54.0 | 58.4 |
| DUT-86-2 | 2449 | 4.97 | 0.57 | 40.9 | 16.0 | 38.0 | 58.4 |
| DUT-86-2/S | 67 | 0.52 | 0.00 | 38.4 | 15.9 | | 58.4 |

[a] Specific surface area. [b] Specific pore volume. [c] Specific micropore volume. [d] Pore diameter. [e] Pore window diameter determined from SAXS pattern fitting. [f] Diameter of pores and of the parent silica particles determined from SAXS pattern fitting.

pores up to 50 nm.[51,52] Nevertheless, both values are much larger for SP-SiC-2 compared to SP-SiC-1. The total pore volumes that are mainly built by mesopores are rather high and are about 2.0 $cm^3\ g^{-1}$. The monodispersity of the large spherical pores is confirmed by small-angle X-ray scattering (SAXS). As shown in Figure 2, an oscillating intensity signal is observed for the silica nanospheres, SNS, the replicated SP-SiC materials, and even the carbide-derived carbons DUT-86. This behavior is typical for spherical scattering bodies (both spherical-shaped particles and pores) in the nanoscale and is only present if the polydispersity index is rather low.[49,50,53] The shift of the first maximum to higher $2\theta$ values indicates the diameter decrease from SNS-X over SP-SiC-X to DUT-86-X (X = 1 or 2). The fitting of those patterns allows determination of the size of the spherical-shaped scattering bodies.[53] The diameters of the parent SNS $d_{SNS,SAXS}$ and the spherical pores $d_{P,SAXS}$ for SP-SiC and DUT-86 are given in Table 1. The intended sizes of the SNS are 40 and 60 nm and, therefore, are in good accordance with the values of 40.8 and 58.4 nm for SNS-1 and SNS-2, respectively. Although the pore diameters decreased to 22.4 and 38.0 nm for the carbide-derived carbons DUT-86-1 and DUT-86-2, respectively, due to shrinkage, it has to be emphasized that the monodispersity can be retained in the nanocasting process to silicon carbide as well as in the chlorine treatment step yielding the uniformly structured carbide-derived carbon materials. Therefore, it is obvious that no structure collapse occurred and that the structure shrinkage is isotropic.

SEM images of the CDCs (Figure 3) reveal the monodispersity, as well. Figure 3E,G shows the high degree of ordering of the spherical pores for DUT-86-1 and DUT-86-2, respectively, due to originally closed-packed silica nanosphere templates and, therefore, the achievement of nanostructured inverse opal CDCs (Figure 3D,F). To the best of our knowledge, such a high degree of perfection in mesopore size distribution and homogeneity has not been achieved before in any hierarchical CDC. Furthermore, the connecting

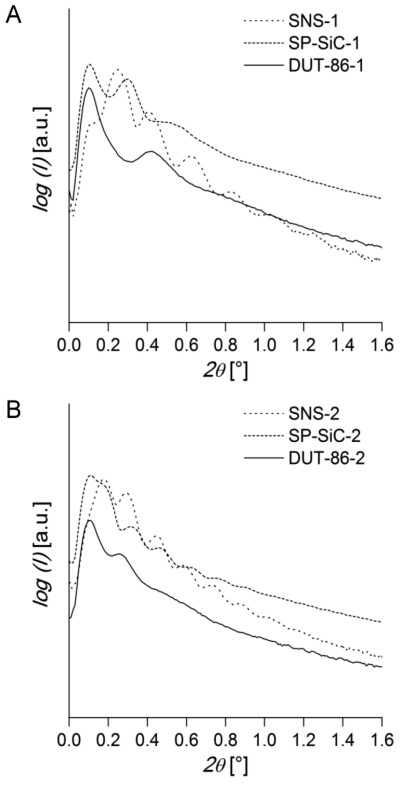


**Figure 2. SAXS patterns of the parent silica nanospheres (SNS-X), nanoporous silicon carbides (SP-SiC-X), and carbide-derived carbon materials (DUT-86-X) for X = 1 (A) or X = 2 (B) with silica sphere size of 40 or 60 nm, respectively (maxima at 0.1° $2\theta$ are caused by a primary beam stop).**

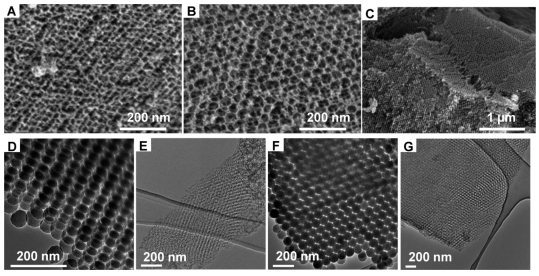


**Figure 3. SEM and TEM images of the carbide-derived carbon materials DUT-86-1 (A,E) and DUT-86-2 (B,C,G) as well as TEM images of the templates SNS-1 (D) and SNS-2 (F).**

windows of the spherical pores are clearly visible for DUT-86-1 and DUT-86-2 in Figure 3A,B, respectively, as well as in the TEM image (Figure S3).

The nitrogen physisorption isotherms of the CDCs in Figure 4A are fully consistent with ideal conservation of the mesopores in the parent silicon carbides SP-SiC-1 and SP-SiC-2. Specific surface areas reach 2400 $m^2\ g^{-1}$ for both DUT-86-1 and DUT-86-2 due to additional formation of micropores. According to Table 1, the sizes of the spherical pores (for PSD, see Figure S2) determined from adsorption branch are in good agreement with the results from SAXS pattern fitting. Furthermore, the window pore sizes decreased during chlorine gas treatment. This was already

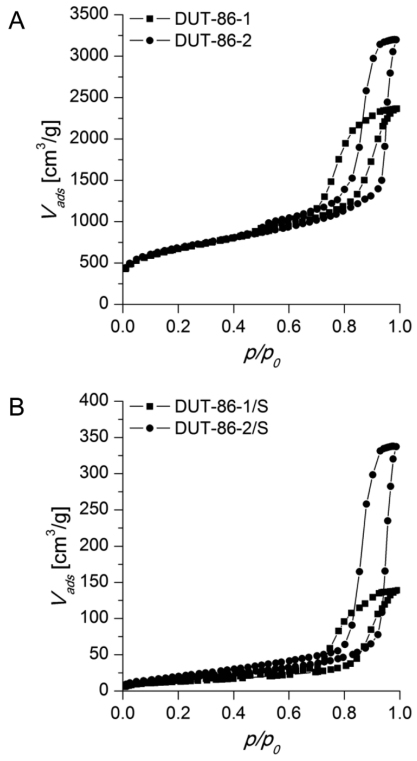


**Figure 4. Nitrogen physisorption isotherms (−196 °C) of the carbide-derived carbon materials DUT-86-1 and DUT-86-2 (A) as well as the carbide-derived carbon/sulfur (CDC/S) composites DUT-86-1/S and DUT-86-2/S (B).**

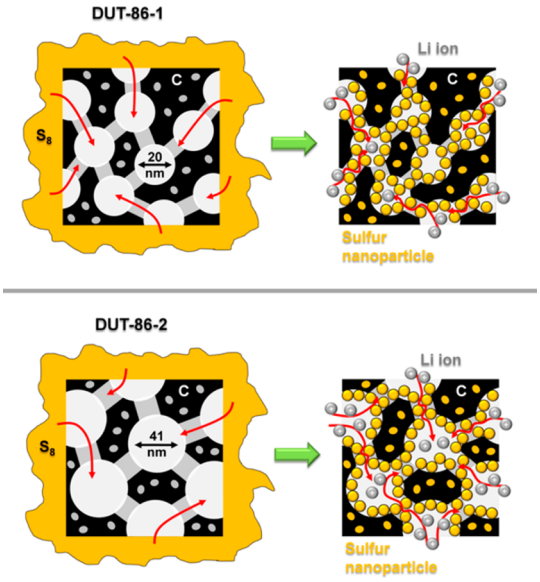


**Figure 5. Schematic representation of the DUT-86-1/S (top) as well as DUT-86-2/S (bottom) nanocomposites before (left) and after (right) melt infiltration of hydrophobic sulfur.**

expected due to the decrease of the spherical pore size without loss of monodispersity observed by SAXS. Accordingly, the window pores become smaller as well during isotropic structural shrinkage. Extraordinary high micro- and mesopore volumes of 3.7 $cm^3\ g^{-1}$ for DUT-86-1 and 5.0 $cm^3\ g^{-1}$ for DUT-86-2 are the unique result. Compared to the silicon carbide ceramics, the micropore volumes are drastically increased (Table 1). However, the micropore ratio is rather low (only 0.5 and 0.6 $cm^3\ g^{-1}$), while large mesopore volumes of 3.2 and 4.4 $cm^3\ g^{-1}$ are present in DUT-86-1 and DUT-86-2, respectively. Hence, DUT-86 stands out due to its unique combination of features combining a high specific surface area, a hierarchical, highly accessible pore system, exceptionally large pore volumes (mainly in the nanopore range from mesopores), and the monodispersity of the spherically shaped nanopores with highly regular inverse opal-like structure. To the best of our knowledge, a carbide-derived carbon structure with comparable properties was not described in the literature so far.

*Carbide-Derived Carbon/Sulfur Composites (DUT-86/S) and Electrode Materials.* Hierarchical porous carbons with high pore volumes as obtained in DUT-86-1 (3.7 $cm^3\ g^{-1}$) and DUT-86-2 (5.0 $cm^3\ g^{-1}$) are ideally suited for lithium−sulfur battery cathodes since large amounts of sulfur can be infiltrated without blocking access of electrolyte to the cathode pores. In fact, we prepared DUT-86-1/S and DUT-86-2/S nanocomposites with 80 wt % sulfur content (equal to 68 wt % active material in total electrode), largely exceeding values reported so far for microporous, mesoporous, as well as bimodal micro-mesoporous carbons.[8,20,22,42,54,55] According to the SEM image of the cathode macrostructure shown in Figure S4A,B, the prepared cathodes exhibit a smooth electrode surface. Neither crack formation nor composite particle delamination was observed, which is highly desirable to achieve a long-term stable porous cathode structure. High-resolution SEM (Figure S4C,D) reveals interparticular porosity, which is necessary for proper electrolyte uptake and homogeneous wetting throughout the active layer. Moreover, a 3D conductive multiwalled carbon nanotube (MWCNT) network as well as binder fibers can be observed. The active layer of the DUT-86-2/S cathode exhibits a thickness of 64 $\mu$m and active material (sulfur) loading of 3.46 $mg_{sulfur}\ cm^{-2}$, corresponding to a cathode density of 0.80 g $cm^{-3}$. In contrast, the DUT-86-1/S cathode is about 12 $\mu$m thinner (52 $\mu$m active layer thickness), although the sulfur loading is approximately the same (3.48 $mg_{sulfur}\ cm^{-2}$), thus indicating a higher cathode density of 0.98 g $cm^{-3}$. The density increase is in good accordance with the higher pore-filling degree of DUT-86-1/S leaving less voids inside the composite particles and consequently in the active layer. This difference in free, accessible pore space influences not only the electrolyte (Li ion) uptake (Figure 5) but also the compensation of up to 78% volume expansion of the active material. Interestingly, the micropore volumes of 0.5 and 0.6 $cm^3\ g^{-1}$ for DUT-86-1 and DUT-86-2, respectively, completely vanished after sulfur uptake (0.0 $cm^3\ g^{-1}$ for both DUT-86-1/S and DUT-86-2/S).

This indicates that a share of up to 26% (DUT-86-1) and 31% (DUT-86-2) of the total is embedded in the micropores, which serves as sulfur storage containers and, due to their high specific surface area, provides intimate electrical contact as well as improved hydrophobic interaction. Accordingly, the specific surface area of the composites are much lower compared to the pristine CDC (Table 1). It should further be noted that the sulfur mass per carbon surface area is similar for both investigated composites (DUT-86-1/S, 1.67 $mg_{sulfur}\ m^{-2}_{carbon}$; DUT-86-2/S, 1.70 $mg_{sulfur}\ m^{-2}_{carbon}$), which enables the characterization of performance parameters linked to the mesopore structure without influences caused by differences in the electrical contact.

After sulfur infiltration, the total pore volume of the DUT-86-2 carbon material was reduced only by 50% from 5.0 to 2.5 $cm^3\ g^{-1}$ (recalculated based on 20 wt % carbon in composite, Figure 4), thus revealing a low pore-filling degree (50 vol %), which is in moderate accordance with the expected theoretical value of 38.6 vol %. This proves the good accessibility of the interconnected, large mesopores of DUT-86-2 even after sulfur uptake. In contrast, the DUT-86-1/S composite exhibits a large decrease in total pore volume from 3.7 to 0.9 $cm^3\ g^{-1}$, indicating a high pore-filling degree of 76 vol %, which is considerably higher than the theoretical predicted value of 52.2 vol %. Exceeding the theoretical values very likely results from pore-clogging effects reducing accessibility of pores during nitrogen physisorption measurements. Those effects are more prominent for DUT-86-1/S proving a more homogeneous sulfur distribution for DUT-86-2/S. According to the PSD of the sulfur infiltrated samples (Figure S2), mesopore coating happens in both composites as is evidenced by the decrease in pore diameter (Table 1). However, the beneficial combination of 41 nm spherical-shaped mesopores, which function as reaction chambers, and 16 nm interconnecting pore windows in DUT-86-2 not only features fast mass transport but also reduces pore blocking upon impregnation with high amounts of sulfur. Thus, upon charge–discharge cycling, the Li ion penetration into the DUT-86-2/S composite particles is preserved, as shown in the schematic model depicted in Figure 5 (bottom). In contrast, the mesopore dimensions of DUT-86-1/S are smaller by the factor of about 2 (diameter of 18 nm, windows of 9 nm size), which might lead to an increased sulfur layer thickness in mesopores compared to DUT-86-2/S. Furthermore, clogging of the 9 nm mesopore windows interconnecting the spherical voids might largely inhibit the accessibility for solvated Li ions (during electrochemical characterzitation) or even small-sized molecules (such as $O_2$ and $N_2$ during TGA and $N_2$ physisorption measurement), as schematically shown in Figure 5 (top).

According to TG analysis, depicted in Figure S5, sulfur was completely infiltrated into the carbon structure. A high sulfur content of 80 wt % was detected in both the DUT-86-1/S and the DUT-86-2/S composites, which is in excellent agreement with the adjusted value. Under oxidative conditions (air), complete combustion of pristine, micrometer-sized sulfur particles (powder) mainly appeared at a temperature higher than 275 °C and terminated at a temperature of about 400 °C. This is surprisingly also the case for nanoparticulate sulfur encapsulated inside the DUT-86-1 pore structure, although nanoparticles are known to exhibit higher reactivity than the bulk material due to their high particle surface-to-volume ratio.[56] The reason therefore is most likely the insufficient accessibility of sulfur particles due to the high pore-filling degree and blockage slowing the reaction kinetics due to mass transport ($O_2$) limitation. In contrast, the combustion of sulfur particles inside DUT-86-2 already appeared at a significantly lower temperature range of 250–350 °C. This shows the easy and rapid diffusion (fast mass transport) of molecules into sulfur-loaded DUT-86-2 caused by the considerably larger mesopore as well as mesopore window size. Since the electrochemical performance is largely influenced by the penetration of solvated Li ions into the composite particles, a similar behavior can be expected with DUT-86-2/S outperforming DUT-86-1/S.

Sulfur is completely X-ray amorphous inside the DUT-86/S composites, as is evidenced by a powder X-ray diffraction (XRD) pattern of the cathode foil shown in Figure S6. The characteristic peaks of bulk sulfur completely vanished after melt infiltration, which confirms the highly dispersed state of sulfur nanoparticles inside the DUT-86 matrix. This nanosize confinement might be supported by the advantageous combination of high surface area micropores (*i.e.*, high contact area between S and C) and monodisperse, spherical mesopores featuring high pore volume (*i.e.*, high sulfur uptake), resulting in homogeneous pore-filling and pore wall coating due to capillary force. The broad peak observed in the powder XRD pattern at about 21° can be assigned to the MWCNT conducting agent, and moreover, a sharp peak at 18.1° from the partially crystalline polytetrafluoroethylene (PTFE) binder can be observed. The homogeneous distribution of sulfur in the composites was further confirmed by EDS mapping (Figure S7).

**Electrochemical Investigations of DUT-86/S Composites.** DUT-86-based composite cathodes exhibit excellent long-term stability over 100 cycles as well as high sulfur utilization up to 70%, nearly reaching the utilization limit of 75% (1256 mAh $g_{sulfur}^{-1}$) predicted by Mikhaylik and Akridge[33] when cycled at room temperature and with a constant rate of *C*/10 (167 mA $g_{sulfur}^{-1}$) (Figure 6). Not only initial capacities as high as 1026 and 1165 mAh $g_{sulfur}^{-1}$ but also reversible capacities of about 760 mAh $g_{sulfur}^{-1}$ (45.5% sulfur utilization) and 860 mAh $g_{sulfur}^{-1}$ (51.4% sulfur utilization) after 100 subsequent charge–discharge cycles are achieved for

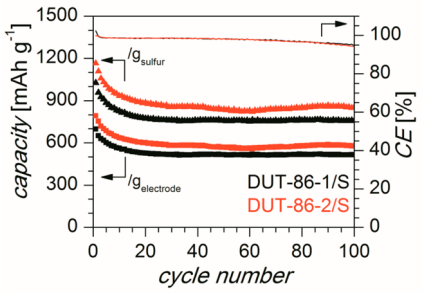


**Figure 6. Achievable capacity, cycling stability, and Coulombic efficiency of the DUT-86/S composites at a current density of *C*/10.**

the DUT-86-1/S and DUT-86-2/S composites, respectively. The performances are reproducible for two separately cycled test cells (Figure 6 and Figure S8). The cathodes were prepared by a solvent-free procedure.[24] The results were obtained by applying electrodes with a high areal sulfur loading of ≈3.5 $mg_{sulfur}$ $cm^{-2}$.

Although high surface area microporous carbon/sulfur composites are interesting from the point of both high sulfur utilization reaching capacities up to 1000−1350 mAh $g_{sulfur}^{-1}$ at moderate rates and excellent active material retention, only microporous carbons possess rather low intraparticular pore volumes (<1 $cm^3$ $g^{-1}$). Accordingly, the sulfur content hosted in the corresponding composites is considerably limited to values below 55 wt $\%_{composite}$.[55,57−60]

Besides the nature of the carbon pore structure, detrimental effects such as diffusion hindrance and pore clogging (slow mass transport) might require even lower sulfur fractions of about 30−45 wt % in the total electrode of a microporous carbon to ensure the high sulfur utilization. To overcome this first of the so-called "two lows" ("two lows" stands for "low sulfur content" and "low sulfur loading"),[61,62] mesoporous carbons can be applied as sulfur hosts, allowing for sulfur fractions as high as 64−85 wt $\%_{composite}$ because of pore volumes largely exceeding 1 $cm^3$ $g^{-1}$. Although the mesoporous carbon/sulfur composites, particularly those with moderate sulfur content, showed good initial sulfur utilization of 60−75% (1000−1250 mAh $g_{sulfur}^{-1}$), much faster capacity fading (32−50% within not more than 100 cycles), compared to composites based on microporous carbons as well as hierarchical carbons such as DUT-86, was observed.[8,21,40,47,63,64] This can be attributed to the considerably reduced specific surface area of mesoporous carbons (≈1000 $m^2$ $g^{-1}$), which directly resulted in a lack of carbon−sulfur contact sites. Accordingly, hierarchical micro-mesoporous carbons such as DUT-86 seem to be beneficial not only due to their high sulfur storage capability in mesopores but also because of numerous electrochemical reaction and polysulfide adsorption sites in micropores. Moreover, the unhindered electrolyte uptake in mesopore voids close to the reaction sites seems highly desirable. In fact, these requirements are perfectly fulfilled by our concept of large mesopore reaction chambers interconnected through small pore windows in combination with micropores, which are incorporated in the mesopore walls. Therefore, initial capacities as high as 1165 mAh $g_{sulfur}^{-1}$ (DUT-86-2/S) and good capacity retention of 74% over 100 cycles were achieved for both DUT-86-1/S and DUT-86-2/S even at a low rate of *C*/10. It should further be noted that the sulfur content was, in both cases, as high as 68 wt % in the total electrode, almost surpassing the first of the "two lows" and thus meeting the commercial requirement of 70 wt %.[65−67] This clearly differentiates our result from earlier publications, where both active material fraction (below 60 wt $\%_{electrode}$) and capacity retention (36−77% after 50−100 cycles) were rather insufficient.[23,41,42,44,68] Consequently, the DUT-86/S cathodes can trigger a vast increase in stable, total electrode weight-related capacities, achieving values of 517 mAh $g_{electrode}^{-1}$ (DUT-86-1/S) and 583 mAh $g_{electrode}^{-1}$ (DUT-86-2/S) after the 100th cycle. More impressively, this stable sulfur utilization can be realized even at sulfur loadings as high as 3.5 $mg_{sulfur}$ $cm^{-2}$, which is a consequence of the tuned pore characteristics of DUT-86. Hence, the areal capacities stabilize at high values of 2.7 mAh $cm^{-2}$ (DUT-86-1/S) and 3.0 mAh $cm^{-2}$ (DUT-86-2/S). This is an important advantage as compared to various reports using low sulfur loadings and areal capacities,[8,20,21,69−72] which in the end leads to insufficient active material to inactive cell component ratios. However, this second of the "two lows" can be overcome by the presented DUT-86/S composites, rendering them promising candidates for a real high energy density lithium−sulfur battery.

The different performances of DUT-86-1 and DUT-86-2 as a conductive carbon matrix in sulfur cathodes is clearly dictated by the difference in sulfur distribution within the mesopore system, which might not only reduce the reactivity of sulfur nanoparticles inside the pores due to formation of agglomerates but also largely inhibit the access of solvated Li ions during discharge. This pore blocking effect in DUT-86-1/S is, consequently, responsible for the reduced electrochemical convertibility of sulfur. In fact, in the first cycle discharge profiles, a suppressed second potential plateau at 2.06−2.09 V *vs* $Li/Li^+$ (Figure 7A) is observed for DUT-86-1/S compared to the second potential plateau of DUT-86-2/S at 2.09−2.11 V *vs* $Li/Li^+$ (Figure 7B), thus demonstrating the difference in initial electrolyte penetration and its detrimental influence on the sulfur utilization. However, after the initial cycle, polysulfides are formed, which remain in a dissolved state inside the pore voids during electrochemical conversion of S to $Li_2S$ and *vice versa*. Since these dissolved intermediates are both highly reactive and mobile, they might trigger a kind of "microshuttle" taking place inside the carbon

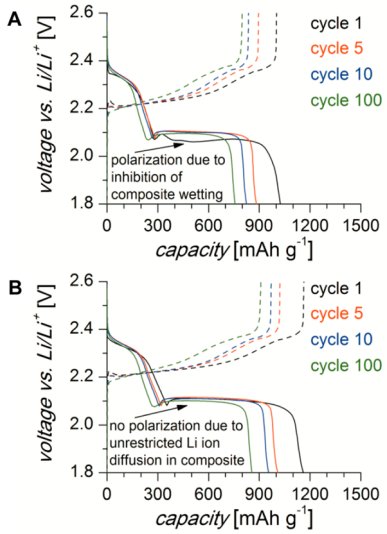


**Figure 7. Charge–discharge profiles for selected cycles (*C*/10) of the cathodes containing DUT-86-X/S for X =1 (A) and X = 2 (B).**

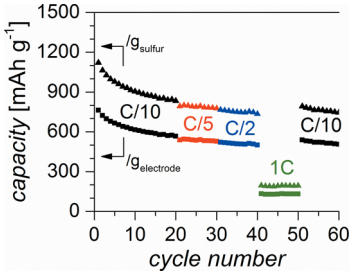


**Figure 8. Cycling stability of the cathodes containing DUT-86-2/S at rates of *C*/10 (0.58 mA cm$^{-2}$), *C*/5 (1.17 mA cm$^{-2}$), *C*/2 (2.92 mA cm$^{-2}$), and 1*C* (5.84 mA cm$^{-2}$).**

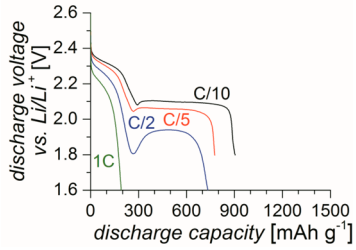


**Figure 9. Discharge profiles of the cathodes containing DUT-86-2/S at variable rates. The 10th cycle at each rate is depicted.**

pores. Thus, redistribution as well as consumption of initially nonreactive (pore) blocking sulfur agglomerates can take place. This activation procedure is most likely the reason for the development of a well-pronounced voltage plateau at 2.09–2.10 V *vs* Li/Li$^+$ for DUT-86-1/S in subsequent cycles. Although this stabilized plateau is comparable to DUT-86-2/S (2.10–2.12 V *vs* Li/Li$^+$), the overall sulfur utilization in DUT-86-1/S (>54%) still lags behind the DUT-86-2/S cathode (>60%).

The pore geometry of DUT-86 is excellently suited to achieve a highly reversible electrochemical transformation of lithium–sulfur species $Li_2S_n$ ($8 \geq n \geq 4$ for soluble and $n$ = 2, 1 for insoluble polysulfides) and sulfur. On the one hand, the spherical-shaped mesopores interconnected *via* small mesopore windows form individual electrochemical reaction chambers, which can suppress active material loss and inhibit polysulfide shuttling through encapsulation. On the other hand, the micropores located in the pore walls can be accessed from the individual reaction chambers, providing intimate, long-lasting (electrical) contact between insulating precipitates and the highly porous carbon. In fact, the sulfur utilization can largely benefit from the improved sulfur mass per carbon surface area ratio (small sulfur particles covering the carbon surface) for both composites (DUT-86-1/S, 1.67 $mg_{sulfur}\,m^{-2}{}_{carbon}$; DUT-86-2/S, 1.70 $mg_{sulfur}\,m^{-2}{}_{carbon}$). Moreover, good sulfur/polysulfide adsorption and reduced shuttling is enabled by the high micropore volume combined with the reaction chamber-like mesopore structure.

*Post mortem* analysis of the charged electrode, which was prepared from DUT-86-2/S after cycling, showed no changes at lower magnifications. The stability of the pore structure was confirmed at higher magnification levels (Figure S9). As a consequence of the generously dimensioned mesopore network of DUT-86-2, which is excellently suited for fast transport of solvated Li ions, high reactivity of homogeneously distributed sulfur nanoparticles, as well as immunity to pore blocking, the DUT-86-2/S cathode shows a good rate performance (Figure 8). At rates of *C*/5 and *C*/2, respectively, stable capacities as high as 800 mAh $g_{sulfur}{}^{-1}$ (544 mAh $g_{electrode}{}^{-1}$) and 766 mAh $g_{sulfur}{}^{-1}$ (521 mAh $g_{electrode}{}^{-1}$) were obtained, although both the sulfur content and loading of the DUT-86-2/S cathodes are high in order to address the "two lows". However, at an even higher rate of 1*C*, corresponding to a current density of 5.84 mA cm$^{-2}$, the discharge capacity suddenly dropped to approximately 195 mAh $g_{sulfur}{}^{-1}$ (133 mAh $g_{electrode}{}^{-1}$). According to the discharge profiles of DUT-86-2/S (Figure 9), this is attributable not only to an increased cell polarization but also, to a great extent, to the slow reaction kinetics of the $Li_2S_2/Li_2S$ deposition in the thick, highly sulfur-loaded active layer. Whereas the first potential plateau is only slightly suppressed, the second potential plateau is degraded to a voltage below the cutoff value (1.6 V *vs* Li/Li$^+$) and, therefore, no longer contributes to the capacity. However, this effect can be reversed by a switch back to a rate of *C*/10 as is indicated by the almost complete recuperation of the extractable capacity in cycle 51–60 (before rate test, 833 mAh $g_{sulfur}{}^{-1}$; after rate test, 791 mAh $g_{sulfur}{}^{-1}$).

## CONCLUSIONS

The use of uniformly sized silica nanospheres in a nanocasting approach to synthesize silicon carbide-derived carbon was investigated. It was demonstrated

that their monodispersity can be transferred to a mesopore system with an inverse opal-like pore arrangement and can be retained even for the CDCs derived by chlorine gas treatment, although isotropic shrinkage took place. Hence, the DUT-86 samples have unique hierarchical pore structure properties characterized by monodisperse spherical mesopores interconnected by smaller windows and microporous walls. Therefore, hierarchical, open-porous CDCs with inverse opal structure and accordingly concave pore walls were obtained. It was shown that the size of the spherical pores as well as the pore windows can be tailored by varying the silica nanosphere size. Spherical pore diameters were adjusted to 18 and 41 nm for DUT-86-1 and DUT-86-2, respectively. The novel carbons have outstanding pore volumes up to 5.0 $cm^3 g^{-1}$ mainly arising from the concave mesopores. This special CDC material can host sulfur for Li−S battery electrodes, resulting in advanced electrochemical performance. The high pore volumes allowed sulfur loadings as high as 80 wt % corresponding to a pore-filling degree of 52% (DUT-86-2), which enabled both high diffusion rates of solvated Li ions and tolerance against the volume expansion during cycling. High initial capacities up to 1165 mAh $g_{sulfur}^{-1}$ render DUT-86 a high-performance sulfur host material in Li−S electrodes, and capacities of 860 mAh $g_{sulfur}^{-1}$ are retained after 100 cycles due to the concave pore geometry inhibiting the capacity loss. The persistent accessibility of sulfur by electrolyte and, beyond that, the long-lasting conductive contact are essential features for the advanced performance.

## EXPERIMENTAL SECTION

**Silica Nanosphere Synthesis.** The silica nanospheres were synthesized by an amino acid controlled method in accordance to Watanabe *et al.*[73] For the seed generation, L-arginine (100 mg; Sigma-Aldrich, ≥98.5%) was dissolved in 100 g of water. After being heated to 70 °C, tetraethyl orthosilicate (TEOS, 5.98 g; Sigma-Aldrich, 98%) was added and the mixture was stirred for 24 h at this temperature. After being cooled, nanospheres were grown. Therefore, a solution containing ethanol (564.9 g), water (220.7 g), and L-arginine (0.783 g) was made, and depending on which particle size was aspired, 15.12 or 5.31 g of seed solution as well as 22.41 or 23.13 g of TEOS were added while stirring to 40 or 60 nm, respectively. The resulting dispersions were stirred for 24 h at 70 °C. After evaporation of the solvent at 80 °C, an oxidation at 600 °C for 2 h was performed and the obtained silica nanospheres were denoted as SNS-1 and SNS-2 for the aimed sizes of 40 and 60 nm, respectively.

**Synthesis of Carbon Materials.** SNS-1 and SNS-2 have been impregnated by incipient wetness with the preceramic polymer SMP-10 (allylhydridopolycarbosilane, Starfire Systems) applying one-third of the mass of the siliceous template. Pyrolysis was performed in argon atmosphere in a tubular aligned furnace under reduced pressure of 800 mbar. After being flushed with Ar, the samples were heated to 1000 °C with 60 K/h and annealed at the final temperature for 2 h. To dissolve the siliceous part, the $SiC/SiO_2$ composites were treated with a mixture of 40 wt % HF, water, and ethanol, one-third each, overnight. Before being washed with ethanol three times, filtration of the solid was performed. The silicon carbide samples SP-SiC-1 and SP-SiC-2 for SNS-1 and SNS-2, respectively, were obtained by finally drying at 80 °C. The subsequent treatment with chlorine gas (mixture of 80 mL/min $Cl_2$ and 70 mL/min Ar) at 1000 °C for 3 h and hydrogen treatment at 600 °C for 1 h was conducted in a quartz tube equipped furnace and resulted in the carbide-derived carbons denoted as DUT-86-1 and DUT-86-2 (DUT = Dresden University of Technology).[16]

**Composite and Electrode Preparation.** The DUT-86/S nanocomposite was prepared following the well-known melt infiltration strategy grinding an appropriate amount of sulfur with the porous carbon host material and subsequent temperature treatment at 155 °C for 12 h in air.[8] Since DUT-86-1 and DUT-86-2 exhibit an extremely high pore volume in the micro-mesopore range of 3.7 $cm^3 g^{-1}$ (DUT-86-1) and 5.0 $cm^3 g^{-1}$ (DUT-86-2), we were able to achieve a high sulfur-to-carbon ratio of 4:1 (by weight) in the nanocomposite. This corresponds to a pore-filling degree of 52.2% (DUT-86-1) and 38.6% (DUT-86-2) based on the density of α-sulfur of 2.07 g $cm^{-3}$, thus leaving substantial void internal pore space to accommodate the volume expansion upon lithium sulfide formation.

For electrochemical characterization, cathodes were prepared from the DUT-86/S nanocomposites following a solvent-free roll-pressing procedure presented in a previous publication.[24,25] First, the DUT-86/S nanocomposite was combined with MWCNT (>95%; Baytubes C 70 P; Bayer MaterialScience) conductive additive, and PTFE (Aldrich) binder in a weight ratio of 85:12:3. This ratio was chosen not only to improve the porosity and wettability of the active layer but also to maximize the sulfur share in the total cathode. After intensive homogenization, the mixture was transferred in a mortar, heated to 125 °C, and sheared by grinding to agglomerate the powdery raw materials. The particle agglomerates (small flakes) were afterward rolled out on a Ceran heating plate to a smooth, mechanically stable cathode film, which was laminated onto a single-sided primed (Electrodag EB-012), expanded aluminum (99.5%; Benmetal−Bender GmbH) current collector. Circular cathode samples (Ø = 12 mm) were punched from the cathode sheet and used without further treatment. All relevant data of the investigated samples are summarized in Table 2.

**Electrochemistry.** For electrochemical characterization, half cells (CR2016 coin-type cells) were assembled in an argon-filled glovebox (<0.1 ppm of $O_2$ and <0.1 ppm of $H_2O$) using the DUT-86/S nanocomposite as the working electrode and elemental lithium as the counter and reference electrode. Cathode and anode were separated by a polypropylene separator and wetted with a sufficient amount of electrolyte, which is 1 M LiTFSI in DME/DOL (1:1, by volume) plus 0.25 M $LiNO_3$ additive. The cells were cycled with a BASYTEC CTS cell test system using

**TABLE 2. Characteristics of the Prepared DUT-86/S Nanocomposite Cathodes**

| cathode component | CDC/S[a] (m/m) | $w_{cathode}(S)$[b] (wt %) | $d_{layer}$[c] (μm) | $y_S$[d] ($mg_{sulfur}$ $cm^{-2}$) | $C_{1.cycle}$ (mAh $g_{sulfur}^{-1}$) | $C_{100.cycle}$ (mAh $g_{sulfur}^{-1}$) |
|---|---|---|---|---|---|---|
| DUT-86-1/S | 1:4 | 68 | 52 | 3.48 | 1026 | 757 |
| DUT-86-2/S | 1:4 | 68 | 64 | 3.46 | 1165 | 860 |

[a] CDC/S composite composition. Cathode composition CDC/S:MWCNT:PTFE (m/m/m) = 85:12:3. [b] Weight ratio of sulfur in the cathode. [c] Active layer thickness. [d] Active material (sulfur) loading.

constant current method at a rate of *C*/10 (167 mA $g_{sulfur}^{-1}$) and ambient temperature to investigate the long-term stability of the DUT-86/S nanocomposite cathode. In order to prevent electrochemical side reactions such as decomposition of $LiNO_3$[74] or electrolyte components, a small voltage window of 1.8−2.6 V *vs* $Li/Li^+$ was adjusted. Furthermore, a rate capability test was performed using variable discharge rates of *C*/10, *C*/5, *C*/2, and 1*C* but a constant charge rate of *C*/10 in order to reduce dendritic lithium growth. To account for increased polarization at high discharge rates (*C*/2 and 1*C*), the voltage window was readjusted to 1.6−2.6 V *vs* $Li/Li^+$.

**Characterization.** The silica nanospheres, silicon carbide samples, and carbide-derived carbons were investigated by SAXS using a Nanostar (Bruker, Cu Kα radiation, $\lambda$ = 0.15405 nm) equipped with a HiStar 2D detector (distance detector−sample = 105 cm), and analyses were performed with the software Scatter.[53] Powder XRD was performed on an X'Pert diffractometer (PANalytical) in Bragg−Brentano geometry (Cu Kα radiation, $\lambda$ = 0.15405 nm). Furthermore, nitrogen physisorption isotherms were measured on a Quadrasorb (Quantachrome) at 77 K after activating the samples, with exception of the carbon−sulfur composites, in vacuum at 423 K overnight. The DUT-86/S composites were activated for at least 48 h in vacuum at ambient temperature. Multipoint BET method was applied for specific surface area calculation using the relative pressure $p/p_0$ range which fulfills the recommendation that $V_{ads}(1 - p/p_0)$ is equal or below the maximum if plotted against $p/p_0$. The specific pore volume $V_P$ was determined at a relative pressure $p/p_0$ of 0.98, and the cumulative pore volume of the quenched solid density functional theory (QSDFT; model for slit, cylindrical and spherical pore geometry using adsorption branch) pore size distribution at a pore size of 2 nm corresponds to the specific micropore volume $V_{micro}$. Pore size distributions were determined according to the BJH method. Samples were investigated by SEM on a DSM982 microscope by Zeiss (for DUT-86) or on JEOL JSM-6610LV (for cathode samples) after being fixed on a carbon pad and being sputtered with gold. Thermal gravimetric analysis of the DUT-86/S composites was performed on a NETZSCH STA 409 in synthetic air (100 mL/min) by heating from ambient temperature up to 1273 K with 5 K/min.

*Conflict of Interest:* The authors declare no competing financial interest.

*Supporting Information Available:* Additional details and figures as mentioned in the text. This material is available free of charge *via* the Internet at http://pubs.acs.org.

## REFERENCES AND NOTES


1. Morris, R. E.; Wheatley, P. S. Gas Storage in Nanoporous Materials. *Angew. Chem., Int. Ed.* **2008**, *47*, 4966–4981.
2. Schlapbach, L.; Zuttel, A. Hydrogen-Storage Materials for Mobile Applications. *Nature* **2001**, *414*, 353–358.
3. Krawiec, P.; Kockrick, E.; Borchardt, L.; Geiger, D.; Corma, A.; Kaskel, S. Ordered Mesoporous Carbide Derived Carbons: Novel Materials for Catalysis and Adsorption. *J. Phys. Chem. C* **2009**, *113*, 7755–7761.
4. Lee, B.; Koo, H.; Park, M.-J.; Lim, B.; Moon, D.; Yoon, K.; Bae, J. Deactivation Behavior of Co/SiC Fischer−Tropsch Catalysts by Formation of Filamentous Carbon. *Catal. Lett.* **2013**, *143*, 18–22.
5. Yushin, G.; Hoffman, E. N.; Barsoum, M. W.; Gogotsi, Y.; Howell, C. A.; Sandeman, S. R.; Phillips, G. J.; Lloyd, A. W.; Mikhalovsky, S. V. Mesoporous Carbide-Derived Carbon with Porosity Tuned for Efficient Adsorption of Cytokines. *Biomaterials* **2006**, *27*, 5755–5762.
6. Presser, V.; Yeon, S.-H.; Vakifahmetoglu, C.; Howell, C. A.; Sandeman, S. R.; Colombo, P.; Mikhalovsky, S.; Gogotsi, Y. Cytokine Removal: Hierarchical Porous Carbide-Derived Carbons for the Removal of Cytokines From Blood Plasma. *Adv. Healthcare Mater.* **2012**, *1*, 682–682.
7. Chmiola, J.; Largeot, C.; Taberna, P.-L.; Simon, P.; Gogotsi, Y. Desolvation of Ions in Subnanometer Pores and Its Effect on Capacitance and Double-Layer Theory. *Angew. Chem., Int. Ed.* **2008**, *47*, 3392–3395.
8. Ji, X.; Lee, K. T.; Nazar, L. F. A Highly Ordered Nanostructured Carbon−Sulphur Cathode for Lithium−Sulphur Batteries. *Nat. Mater.* **2009**, *8*, 500–506.
9. Candelaria, S. L.; Shao, Y.; Zhou, W.; Li, X.; Xiao, J.; Zhang, J.-G.; Wang, Y.; Liu, J.; Li, J.; Cao, G. Nanostructured Carbon for Energy Storage and Conversion. *Nano Energy* **2012**, *1*, 195–220.
10. Lee, J.; Kim, J.; Hyeon, T. Recent Progress in the Synthesis of Porous Carbon Materials. *Adv. Mater.* **2006**, *18*, 2073–2094.
11. Rodríguez-Reinoso, F.; Molina-Sabio, M.; González, M. T. The Use of Steam and $CO_2$ as Activating Agents in the Preparation of Activated Carbons. *Carbon* **1995**, *33*, 15–23.
12. Oschatz, M.; Borchardt, L.; Senkovska, I.; Klein, N.; Leistner, M.; Kaskel, S. Carbon Dioxide Activated Carbide-Derived Carbon Monoliths as High Performance Adsorbents. *Carbon* **2013**, *56*, 139–145.
13. Wang, J.; Kaskel, S. KOH Activation of Carbon-Based Materials for Energy Storage. *J. Mater. Chem.* **2012**, *22*, 23710–23725.
14. Lu, A. H.; Schüth, F. Nanocasting: A Versatile Strategy for Creating Nanostructured Porous Materials. *Adv. Mater.* **2006**, *18*, 1793–1805.
15. Presser, V.; Heon, M.; Gogotsi, Y. Carbide-Derived Carbons—From Porous Networks to Nanotubes and Graphene. *Adv. Funct. Mater.* **2011**, *21*, 810–833.
16. Oschatz, M.; Borchardt, L.; Thommes, M.; Cychosz, K. A.; Senkovska, I.; Klein, N.; Frind, R.; Leistner, M.; Presser, V.; Gogotsi, Y.; *et al.* Carbide-Derived Carbon Monoliths with Hierarchical Pore Architectures. *Angew. Chem., Int. Ed.* **2012**, *51*, 7577–7580.
17. Oschatz, M.; Kockrick, E.; Rose, M.; Borchardt, L.; Klein, N.; Senkovska, I.; Freudenberg, T.; Korenblit, Y.; Yushin, G.; Kaskel, S. A Cubic Ordered, Mesoporous Carbide-Derived Carbon for Gas and Energy Storage Applications. *Carbon* **2010**, *48*, 3987–3992.
18. Oschatz, M.; Borchardt, L.; Pinkert, K.; Thieme, S.; Lohe, M. R.; Hoffmann, C.; Benusch, M.; Wisser, F. M.; Ziegler, C.; Giebeler, L.; *et al.* Hierarchical Carbide-Derived Carbon Foams with Advanced Mesostructure as a Versatile Electrochemical Energy-Storage Material. *Adv. Energy Mater.* **2014**, *4*, 1300645/1–1300645/9.
19. Tripathi, P. K.; Liu, M.; Gan, L.; Qian, J.; Xu, Z.; Zhu, D.; Rao, N. N. High Surface Area Ordered Mesoporous Carbon for High-Level Removal of Rhodamine B. *J. Mater. Sci.* **2013**, *48*, 8003–8013.
20. Liang, C.; Dudney, N. J.; Howe, J. Y. Hierarchically Structured Sulfur/Carbon Nanocomposite Material for High-Energy Lithium Battery. *Chem. Mater.* **2009**, *21*, 4724–4730.
21. Li, X.; Cao, Y.; Qi, W.; Saraf, L. V.; Xiao, J.; Nie, Z.; Mietek, J.; Zhang, J.-G.; Schwenzer, B.; Liu, J. Optimization of Mesoporous Carbon Structures for Lithium−Sulfur Battery Applications. *J. Mater. Chem.* **2011**, *21*, 16603–16610.
22. Jayaprakash, N.; Shen, J.; Moganty, S. S.; Corona, A.; Archer, L. A. Porous Hollow Carbon@Sulfur Composites for High-Power Lithium−Sulfur Batteries. *Angew. Chem.* **2011**, *123*, 6026–6030.
23. Chen, S.-R.; Zhai, Y.-P.; Xu, G.-L.; Jiang, Y.-X.; Zhao, D.-Y.; Li, J.-T.; Huang, L.; Sun, S.-G. Ordered Mesoporous Carbon/Sulfur Nanocomposite of High Performances as Cathode for Lithium−Sulfur Battery. *Electrochim. Acta* **2011**, *56*, 9549–9555.
24. Thieme, S.; Brueckner, J.; Bauer, I.; Oschatz, M.; Borchardt, L.; Althues, H.; Kaskel, S. High Capacity Micro-mesoporous Carbon−Sulfur Nanocomposite Cathodes with Enhanced Cycling Stability Prepared by a Solvent-Free Procedure. *J. Mater. Chem. A* **2013**, *1*, 9225–9234.
25. Oschatz, M.; Thieme, S.; Borchardt, L.; Lohe, M. R.; Biemelt, T.; Brueckner, J.; Althues, H.; Kaskel, S. A New Route for the Preparation of Mesoporous Carbon Materials with High Performance in Lithium−Sulphur Battery Cathodes. *Chem. Commun.* **2013**, *49*, 5832–5834.
26. Kim, J.; Lee, D.-J.; Jung, H.-G.; Sun, Y.-K.; Hassoun, J.; Scrosati, B. An Advanced Lithium−Sulfur Battery. *Adv. Funct. Mater.* **2013**, *23*, 1076–1080.

27. Woo, S.-W.; Dokko, K.; Nakano, H.; Kanamura, K. Incorporation of Polyaniline into Macropores of Three-Dimensionally Ordered Macroporous Carbon Electrode for Electrochemical Capacitors. *J. Power Sources* **2009**, *190*, 596–600.
28. Qiao, Z.-A.; Guo, B.; Binder, A. J.; Chen, J.; Veith, G. M.; Dai, S. Controlled Synthesis of Mesoporous Carbon Nanostructures *via* a "Silica-Assisted" Strategy. *Nano Lett.* **2013**, *13*, 207–212.
29. Li, H.; Chang, L.; Wang, J.; Yang, L.; Song, Y. A Colorful Oil-Sensitive Carbon Inverse Opal. *J. Mater. Chem.* **2008**, *18*, 5098–5103.
30. Yamada, Y.; Ishii, M.; Nakamura, T.; Yano, K. Artificial Black Opal Fabricated from Nanoporous Carbon Spheres. *Langmuir* **2010**, *26*, 10044–10049.
31. Fan, W.; Snyder, M. A.; Kumar, S.; Lee, P.-S.; Yoo, W. C.; McCormick, A. V.; Lee Penn, R.; Stein, A.; Tsapatsis, M. Hierarchical Nanofabrication of Microporous Crystals with Ordered Mesoporosity. *Nat. Mater.* **2008**, *7*, 984–991.
32. Wang, S.; Zhao, Q.; Wei, H.; Wang, J.-Q.; Cho, M.; Cho, H. S.; Terasaki, O.; Wan, Y. Aggregation-Free Gold Nanoparticles in Ordered Mesoporous Carbons: Toward Highly Active and Stable Heterogeneous Catalysts. *J. Am. Chem. Soc.* **2013**, *135*, 11849–11860.
33. Mikhaylik, Y. V.; Akridge, J. R. Polysulfide Shuttle Study in the Li/S Battery System. *J. Electrochem. Soc.* **2004**, *151*, A1969–A1976.
34. Mikhaylik, Y.; Kovalev, I.; Schock, R.; Kumaresan, K.; Xu, J.; Affinito, J. High Energy Rechargeable Li–S Cells for EV Application. Status, Remaining Problems and Solutions. *ECS Trans.* **2010**, *25*, 23–34.
35. De-Leon, S. *Lithium Sulfur & Li-Metal Rechargeable Batteries, Technology, Applications & Market Review 2013 Version 2*; Shmuel De-Leon Energy, Ltd.: Hod HaSharon, Israel, 2013; pp 1–99.
36. Kumaresan, K.; Mikhaylik, Y.; White, R. E. A Mathematical Model for a Lithium–Sulfur Cell. *J. Electrochem. Soc.* **2008**, *155*, A576–A582.
37. Barchasz, C.; Molton, F.; Duboc, C.; Leprêtre, J.-C.; Patoux, S.; Alloin, F. Lithium/Sulfur Cell Discharge Mechanism: An Original Approach for Intermediate Species Identification. *Anal. Chem.* **2012**, *84*, 3973–3980.
38. Cheon, S.-E.; Choi, S.-S.; Han, J.-S.; Choi, Y.-S.; Jung, B.-H.; Lim, H. S. Capacity Fading Mechanisms on Cycling a High-Capacity Secondary Sulfur Cathode. *J. Electrochem. Soc.* **2004**, *151*, A2067–A2073.
39. Choi, Y. S.; Kim, S.; Choi, S. S.; Han, J. S.; Kim, J. D.; Jeon, S. E.; Jung, B. H. Effect of Cathode Component on the Energy Density of Lithium–Sulfur Battery. *Electrochim. Acta* **2004**, *50*, 833–835.
40. Zheng, J.; Gu, M.; Wagner, M. J.; Hays, K. A.; Li, X.; Zuo, P.; Wang, C.; Zhang, J.-G.; Liu, J.; Xiao, J. Revisit Carbon/Sulfur Composite for Li–S Batteries. *J. Electrochem. Soc.* **2013**, *160*, A1624–A1628.
41. He, G.; Ji, X.; Nazar, L. High "C" Rate Li–S Cathodes: Sulfur Imbibed Bimodal Porous Carbons. *Energy Environ. Sci.* **2011**, *4*, 2878–2883.
42. Schuster, J.; He, G.; Mandlmeier, B.; Yim, T.; Lee, K. T.; Bein, T.; Nazar, L. F. Spherical Ordered Mesoporous Carbon Nanoparticles with High Porosity for Lithium–Sulfur Batteries. *Angew. Chem., Int. Ed.* **2012**, *51*, 3591–3595.
43. Wang, D.-W.; Zhou, G.; Li, F.; Wu, K.-H.; Lu, G. Q.; Cheng, H.-M.; Gentle, I. R. A Microporous–Mesoporous Carbon with Graphitic Structure for a High-Rate Stable Sulfur Cathode in Carbonate Solvent-Based Li–S Batteries. *Phys. Chem. Chem. Phys.* **2012**, *14*, 8703–8710.
44. Lee, J. T.; Zhao, Y.; Thieme, S.; Kim, H.; Oschatz, M.; Borchardt, L.; Magasinski, A.; Cho, W.-I.; Kaskel, S.; Yushin, G. Sulfur-Infiltrated Micro- and Mesoporous Silicon Carbide-Derived Carbon Cathode for High-Performance Lithium Sulfur Batteries. *Adv. Mater.* **2013**, *25*, 4573–4579.
45. Yang, Y.; Yu, G.; Cha, J. J.; Wu, H.; Vosgueritchian, M.; Yao, Y.; Bao, Z.; Cui, Y. Improving the Performance of Lithium–Sulfur Batteries by Conductive Polymer Coating. *ACS Nano* **2011**, *5*, 9187–9193.
46. Lee, K. T.; Black, R.; Yim, T.; Ji, X.; Nazar, L. F. Surface-Initiated Growth of Thin Oxide Coatings for Li–Sulfur Battery Cathodes. *Adv. Energy Mater.* **2012**, *2*, 1490–1496.
47. Li, D.; Han, F.; Wang, S.; Cheng, F.; Sun, Q.; Li, W.-C. High Sulfur Loading Cathodes Fabricated Using Peapodlike, Large Pore Volume Mesoporous Carbon for Lithium–Sulfur Battery. *ACS Appl. Mater. Interfaces* **2013**, *5*, 2208–2213.
48. Kim, H.; Lee, J. T.; Lee, D.-C.; Magasinski, A.; Cho, W.-i.; Yushin, G. Plasma-Enhanced Atomic Layer Deposition of Ultrathin Oxide Coatings for Stabilized Lithium–Sulfur Batteries. *Adv. Energy Mater.* **2013**, *3*, 1308–1315.
49. Hoffmann, C.; Biemelt, T.; Seifert, A.; Pinkert, K.; Gemming, T.; Spange, S.; Kaskel, S. Polymer-Derived Nanoporous Silicon Carbide with Monodisperse Spherical Pores. *J. Mater. Chem.* **2012**, *22*, 24841–24847.
50. Hoffmann, C.; Biemelt, T.; Lohe, M. R.; Rümmeli, M. H.; Kaskel, S. Nanoporous and Highly Active Silicon Carbide Supported $CeO_2$-Catalysts for the Methane Oxidation Reaction. *Small* **2013**, *10*, 316–322.
51. Sing, K. S. W.; Everett, D. H.; Haul, R. A. W.; Moscou, L.; Pierotti, R. A.; Rouquerol, J.; Siemieniewska, T. Reporting Physisorption Data for Gas/Solid Systems with Special Reference to the Determination of Surface Area and Porosity (Recommendations 1984). *Pure Appl. Chem.* **1985**, *57*, 603–619.
52. Rouquerol, J.; Avnir, D.; Fairbridge, C. W.; Everett, D. H.; Haynes, J. H.; Pernicone, N.; Ramsay, J. D. F.; Sing, K. S. W.; Unger, K. K. Recommendations for the Characterization of Porous Solids. *Pure Appl. Chem.* **1994**, *66*, 1739–1758.
53. Förster, S.; Fischer, S.; Zielske, K.; Schellbach, C.; Sztucki, M.; Lindner, P.; Perlich, J. Calculation of Scattering-Patterns of Ordered Nano- and Mesoscale Materials. *Adv. Colloid Interface Sci.* **2011**, *163*, 53–83.
54. Lai, C.; Gao, X. P.; Zhang, B.; Yan, T. Y.; Zhou, Z. Synthesis and Electrochemical Performance of Sulfur/Highly Porous Carbon Composites. *J. Phys. Chem. C* **2009**, *113*, 4712–4716.
55. Zhang, B.; Qin, X.; Li, G. R.; Gao, X. P. Enhancement of Long Stability of Sulfur Cathode by Encapsulating Sulfur Into Micropores of Carbon Spheres. *Energy Environ. Sci.* **2010**, *3*, 1531–1537.
56. Parak, W. J.; Manna, L.; Simmel, F. C.; Gerion, D.; Alivisatos, P. Quantum Dots. In *Nanoparticles*; Wiley-VCH: Weinheim, Germany, 2010; pp 3–47.
57. Elazari, R.; Salitra, G.; Garsuch, A.; Panchenko, A.; Aurbach, D. Sulfur-Impregnated Activated Carbon Fiber Cloth as a Binder-Free Cathode for Rechargeable Li–S Batteries. *Adv. Mater.* **2011**, *23*, 5641–5644.
58. Rao, M.; Li, W.; Cairns, E. J. Porous Carbon–Sulfur Composite Cathode for Lithium/Sulfur Cells. *Electrochem. Commun.* **2012**, *17*, 1–5.
59. Zhang, W.; Qiao, D.; Pan, J.; Cao, Y.; Yang, H.; Ai, X. A $Li^+$-Conductive Microporous Carbon–Sulfur Composite for Li–S Batteries. *Electrochim. Acta* **2013**, *87*, 497–502.
60. Xin, S.; Gu, L.; Zhao, N.-H.; Yin, Y.-X.; Zhou, L.-J.; Guo, Y.-G.; Wan, L.-J. Smaller Sulfur Molecules Promise Better Lithium–Sulfur Batteries. *J. Am. Chem. Soc.* **2012**, *134*, 18510–18513.
61. Miao, L.-X.; Wang, W.-K.; Wang, A.-B.; Yuan, K.-G.; Yang, Y.-S. A High Sulfur Content Composite with Core–Shell Structure as Cathode Material for Li–S Batteries. *J. Mater. Chem. A* **2013**, *1*, 11659–11664.
62. Wang, M.; Wang, W.; Wang, A.; Yuan, K.; Miao, L.; Zhang, X.; Huang, Y.; Yu, Z.; Qiu, J. A Multi-Core–Shell Structured Composite Cathode Material with a Conductive Polymer Network for Li–S Batteries. *Chem. Commun.* **2013**, *49*, 10263–10265.
63. Zhang, C.; Wu, H. B.; Yuan, C.; Guo, Z.; Lou, X. W. Confining Sulfur in Double-Shelled Hollow Carbon Spheres for Lithium–Sulfur Batteries. *Angew. Chem., Int. Ed.* **2012**, *51*, 9592–9595.
64. Ma, G.; Wen, Z.; Jin, J.; Lu, Y.; Rui, K.; Wu, X.; Wu, M.; Zhang, J. Enhanced Performance of Lithium Sulfur Battery with Polypyrrole Warped Mesoporous Carbon/Sulfur Composite. *J. Power Sources* **2014**, *254*, 353–359.

65. Kolosnitsyn, V.; Karaseva, E. Lithium–Sulphur Battery with High Specific Energy. Patent Appl. GB2430542A, March 28, 2007.
66. Kolosnitsyn, V.; Karaseva, E. Lithium Secondary Battery for Operation over a Range of Temperatures. Patent Appl. US20070281210A1, December 6, 2007.
67. Zhang, S. S. Liquid Electrolyte Lithium/Sulfur Battery: Fundamental Chemistry, Problems, and Solutions. *J. Power Sources* **2013**, *231*, 153–162.
68. Wang, X.; Fang, X.; Guo, X.; Wang, Z.; Chen, L. Sulfur in Hierarchically Pore-Structured Carbon Pillars as Cathode Material for Lithium–Sulfur Batteries. *Electrochim. Acta* **2013**, *97*, 238–243.
69. Wang, H.; Yang, Y.; Liang, Y.; Robinson, J. T.; Li, Y.; Jackson, A.; Cui, Y.; Dai, H. Graphene-Wrapped Sulfur Particles as a Rechargeable Lithium–Sulfur Battery Cathode Material with High Capacity and Cycling Stability. *Nano Lett.* **2011**, *11*, 2644–2647.
70. Zhang, S. Improved Cyclability of Liquid Electrolyte Lithium/Sulfur Batteries by Optimizing Electrolyte/Sulfur Ratio. *Energies* **2012**, *5*, 5190–5197.
71. Evers, S.; Nazar, L. F. Graphene-Enveloped Sulfur in a One Pot Reaction: A Cathode with Good Coulombic Efficiency and High Practical Sulfur Content. *Chem. Commun.* **2012**, *48*, 1233–1235.
72. Zhao, M.-Q.; Zhang, Q.; Huang, J.-Q.; Tian, G.-L.; Nie, J.-Q.; Peng, H.-J.; Wei, F. Unstacked Double-Layer Templated Graphene for High-Rate Lithium–Sulphur Batteries. *Nat. Commun.* **2014**, *5*, 4410/1–4410/8.
73. Watanabe, R.; Yokoi, T.; Kobayashi, E.; Otsuka, Y.; Shimojima, A.; Okubo, T.; Tatsumi, T. Extension of Size of Monodisperse Silica Nanospheres and Their Well-Ordered Assembly. *J. Colloid Interface Sci.* **2011**, *360*, 1–7.
74. Zhang, S. S. Role of $LiNO_3$ in Rechargeable Lithium/Sulfur Battery. *Electrochim. Acta* **2012**, *70*, 344–348.